

IMECE2006-15291

**FLEXURE-BASED TWO DEGREE-OF-FREEDOM LEGS FOR WALKING
MICROROBOTS**

Ankur M. Mehta

Berkeley Sensor and Actuator Center
Department of Electrical Engineering
University of California
Berkeley, California 94720-1774
Email: mehtank@eecs.berkeley.edu

Kristofer S. J. Pister

Berkeley Sensor and Actuator Center
Department of Electrical Engineering
University of California
Berkeley, California 94720-1774

ABSTRACT

This work examines the design of legs for a walking microrobot. The parameterized force-displacement relationships of planar serpentine flexure-based two degree-of-freedom legs are analyzed. An analytical model based on Euler-Bernoulli beam theory is developed to explore the design space, and is subsequently refined to include contact between adjacent beams. This is used to determine a successful leg geometry given dimensional constraints and actuator limitations. Standard comb drive actuators that output 100 μN of force over a 15 μm bi-directional throw are shown able to drive a walking gait with three legs on a 1 cm^2 silicon die microrobot. If the comb drive suspensions cannot withstand the generated reaction moments, an alternate pivot-based leg linkage is proposed.

1 INTRODUCTION

Microscale devices has been an area of heavy research for decades now, but only recently has there been much progress towards complete microscale systems. The integration of sensing, processing, and communication now allows autonomous sensor nodes in a distributed network. However, these are still passive systems, capable of interacting with the environment only within the area they have been placed. A key element lacking in these microsystems is mobility. Microrobots coupling a method of locomotion with such a node can be conceived. These integrated autonomous microrobots can be useful in a variety of surveillance, exploration, and rescue tasks.

There are many proposed methods to enable microscale locomotion. Research is underway to develop shuffling, flying, and jumping microrobots. Shuffling robots rely on specific properties of the ground on which they move. Patterned active substrates have enabled some of the smallest mobile devices, but do not allow a fully integrated system and are incapable of interacting with more general environments [1]. Flying is primarily useful for traveling large distances, and often incorporates high energy density hydrocarbon fuels for power [2]. However, such systems are necessarily complex and often lack precise positioning. Jumping microrobots take their cue from insects in nature, storing energy in an elastomer and releasing it quickly to launch them several times their body length [3]. These systems too lack precise positioning, generally using a random walk approach.

This work focuses on enabling walking motion in MEMS microrobots. Walking refers to a method in which the weight of the robot is supported on one set of legs as another set is moved forward off the ground, then transferred to the second set. The legs follow periodic non-slip motions. This approach was chosen because it enables precise positioning and steering of microrobots on passive surfaces. It can also be effectively powered by high voltage, low current solar cells. The primary limitation in walking effectiveness is the step size of the legs, requiring surfaces to have roughness features smaller than that size scale.

A walking motion requires at least two dimensions of travel at the foot: the “horizontal” translation which drives the robot forward, and the “vertical” translation which lifts the leg and/or robot from the ground so it can move into position for the next stride. This generally calls for a leg system with at least two degrees of freedom. A walking microrobot with two single degree-of-freedom legs was previously developed in [4]. It used solar cells for power, with onboard processing for control. However, it failed for several reasons. It used a complicated multi-step fabrication process that was often finicky and unreliable. Also, the actuators driving the legs were incapable of providing the force required to drag the robot body behind it.

This work begins to examine a walking microrobot that can overcome these problems. In particular, the primary consideration is a simpler fabrication process. Avoiding heavy process development allows for more attention to mechanism design, with quicker turnaround of design iterations. The design focuses on planar two degree-of-freedom trapezoidal legs assembled out of plane to generate the walking motion, and proceeds with a mechanical analysis of the linkages required for such a leg.

2 MEMS FABRICATION

A significant consideration in designing microscale systems is how such a design can then be implemented. Microelectromechanical systems (MEMS) technology employs a variety of semiconductor processing techniques to create mechanical devices. However, due to process abilities and limitations, both device and process design must be considered and developed simultaneously. There is often a trade-off in designing MEMS devices between functionality and process steps. As more complex mechanical elements are desired, higher complexity processing is needed. Process development is time consuming and expensive, and can draw research focus away from device design. Thus, simple but versatile process steps are desired.

The process used in this work is a one mask SOI process. The mask is used to pattern photoresist through which the device layer on an SOI wafer is etched. This results in a constant-thickness two dimensional pattern in the device layer. The buried oxide is then etched away, undercutting the features in the device layer and releasing some structures completely. Many structures can be made using this process, including a variety of actuators and linkages. Comb drives, gap closers, and thermal actuators are all possible, along with two dimensional transmissions that can enable more complex actuators such as inchworm motors.

While allowing for a rich set of planar geometries, the single mask SOI process is severely limited by being constrained to two dimensions. One way of overcoming this limitation is by incorporating a post-processing assembly step, as explained in [5]. Structures released in the device layer can be picked up, rotated out of plane, and assembled into clamps in the device layer. This “pick and place microassembly” process was de-

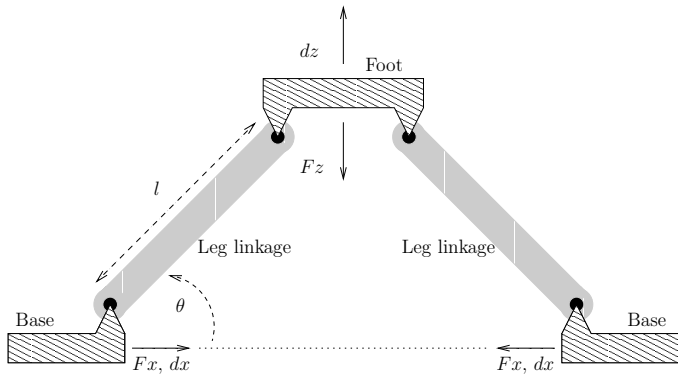


Figure 1. An ideal trapezoidal leg consists of rigid members connected by free pivots.

signed to replace numerous cleanroom fabrication steps with a single assembly step to create three dimensional structures.

3 TRAPEZOIDAL LEG

The key mechanism presented in this paper is a two dimensional trapezoidal leg, driven by two independently actuated linear comb drives. A schematic of such a leg is shown in Fig. 1. The leg is attached to each comb drive at its bases, which move horizontally. The bases are connected by linkages to the foot, which provides the output motion. It is this linkage that will be examined here in an attempt to effect the desired walking motion at the foot.

3.1 Leg Linkage

An ideal linkage would consist of rigid beams connected by ideal pivots to allow free rotation of adjacent members, as in Fig. 1. For such a design, the only design parameters impacting the behavior are the length l of the linking beam and its angle θ with respect to the line of actuation. However, pivots in general are difficult to fabricate in planar MEMS processes, especially in the single layer SOI processes mentioned above.

As an alternative, flexible beams can be used to provide the structure with the requisite compliance. Due to the stiffness of silicon, a single beam flexure requires excessive force to generate the desired motion, so a serpentine trifold beam design is used (Fig. 2). In addition to the length l and angle θ , the design space now includes as the width w of the beams and the spacing d between segments of the folded beam.

A folded beam flexure can be used to implement an effective pivot to more closely approximate a real pivot. In a single layer SOI device, a hinge becomes a cylinder-in-socket pivot. To keep the cylinder from falling out of the socket, a loose serpentine spring is used to connect the pieces, as in Fig. 3. The friction in the pivot between the moving pieces can be drastically reduced

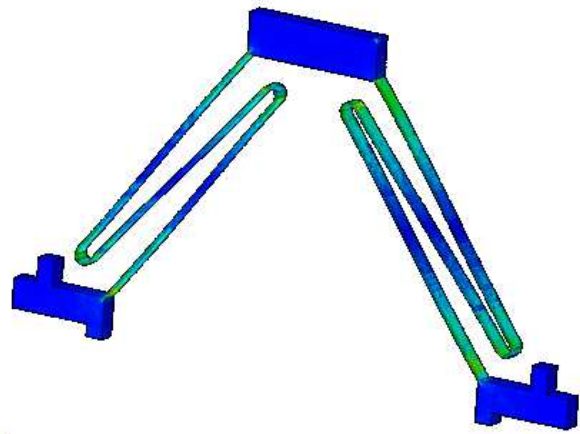


Figure 2. A model of an assemblable trifold flexural beam.

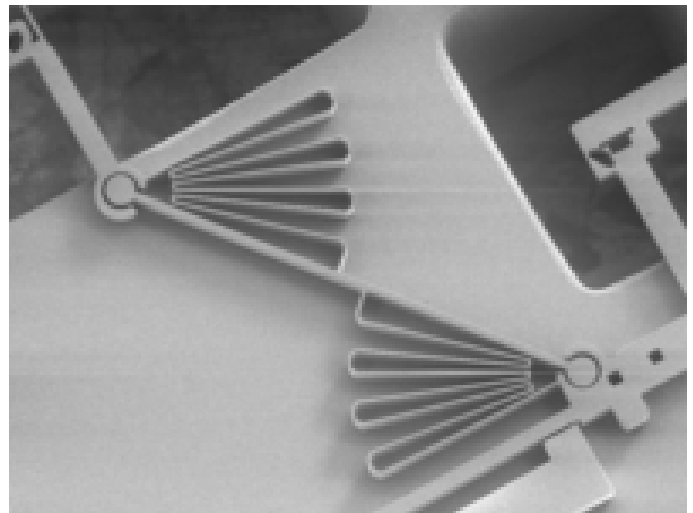


Figure 3. Pivots can be approximated by planar cylinder-in-socket joints, with the segments held together by long serpentine springs.

by replacing the cylinder-in-socket pivot with a knife-edge pivot, as in Fig. 4.

3.2 Foot motion

The output motion at the foot is controlled by the comb drives attached to the bases. Common mode operation of these comb drives results in the foot being actuated horizontally, while differential mode operation causes vertical motion, as in Fig. 5. The leg acts as a transmission generating a periodic two-dimensional cyclic motion from out-of-phase actuation of the two comb drives. A similar actuator is seen in [6]. In turn, an-

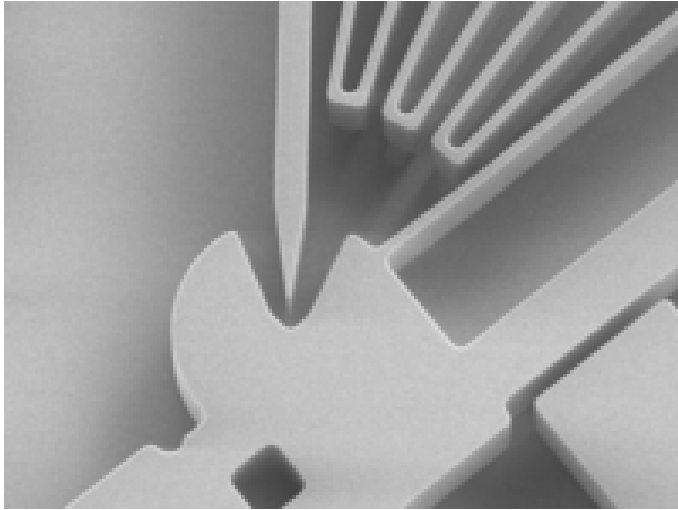


Figure 4. Knife-edge pivots minimize frictional forces impeding rotation.

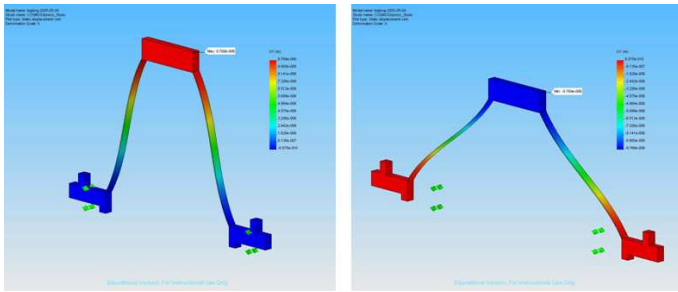


Figure 5. The figure on the left shows the leg with the independent bases actuated in, raising the foot, while the figure on the right shows the bases actuated out, lowering the foot. If both bases are actuated in the same direction, the foot simply translates.

tiphase operation of a pair of similar legs can be used to propel a robot forward, as seen in Fig. 6. Each footstep sends the robot forward the full throw of the comb drives, thus relating the speed of the robot to the frequency at which the actuators are driven. The height the foot is lifted each step sets the maximum roughness of the surface the robot can navigate.

In designing such a leg, there are four quantities that need to be considered. The forces F_x and F_z are applied to the base and foot, respectively, which undergo displacements d_x and d_z . It is the relationships between these that define the performance of the motion system. The comb drive actuators must provide sufficient force F_x over their range of motion d_x to be able to lift the distributed weight of the robot F_z a distance d_z . In an ideal leg, with rigid members and ideal pivots, these relationships are easily determined by geometry:

$$F_z = F_x \tan \theta, \quad (1)$$

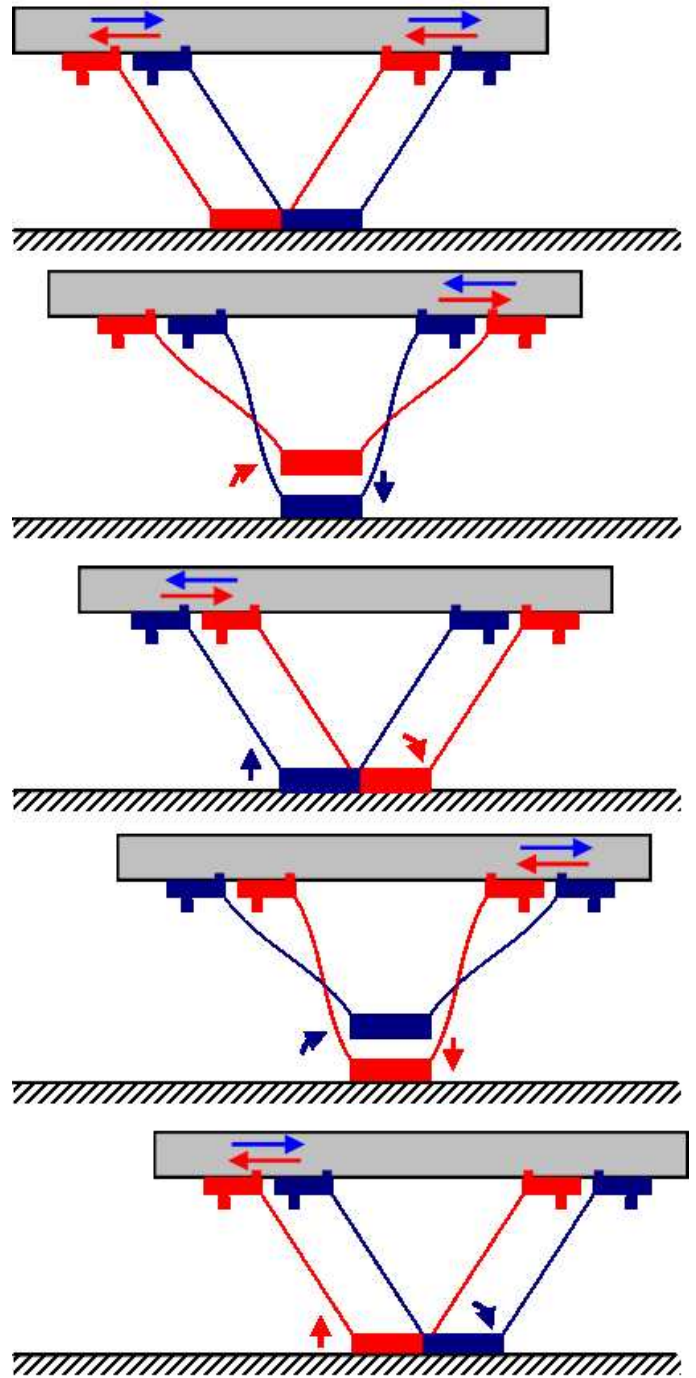


Figure 6. Two such legs operating out of phase can be used to propel a robot forward along smooth ground.

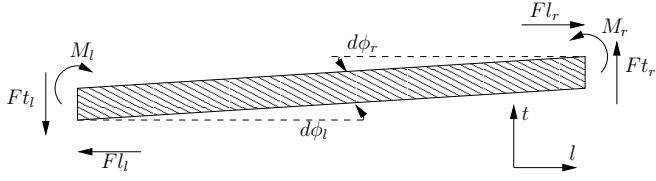


Figure 7. A simple beam with loading only at the edges

$$d_z = -d_x / \tan \theta. \quad (2)$$

However, with the flexures or non-ideal pivots described above, the relationships are not so simple, and cross terms enter the equations. It is then important to know what is being designed for. As a starting point, standard library comb drives are used. At 50V actuation voltage, they are capable of applying up to $100\mu\text{N}$ force over $15\mu\text{m}$ of bi-directional travel. If three legs are being used to support a 1cm^2 microrobot die from a $300\mu\text{m}$ thick wafer, each leg must support about $250\mu\text{N}$, or alternately, each linkage must provide up to $125\mu\text{N}$ vertical force.

4 LINEAR BEAM THEORY

The folded beam structures comprise individual simply loaded Euler-Bernoulli beams connected at their ends. In this first order approximation, a set of linear relations can be defined between displacements, forces, and moments at opposite ends of each simple beam. Consider a long thin member, loaded only at the edges but free everywhere along its length, of length l , Young's modulus E , and cross sectional inertia $I (= tw^3/12$ for a rectangular cross section of width w and out of plane thickness t). Adopting a sign convention as shown in Fig. 7, the applied loads at either end in the directions indicated can be related to the linear and angular displacements of the edges:

$$dl_r = dl_l + ld\phi_l + \frac{l^2}{2EI}M_l - \frac{l^3}{6EI}Fl_l, \quad (3)$$

$$d\phi_r = d\phi_l + \frac{l}{EI}M_l - \frac{l^2}{2EI}Fl_l, \quad (4)$$

$$M_r = M_l - lFl_l, \quad (5)$$

$$Fl_r = Fl_l. \quad (6)$$

There are no longitudinal deflections or forces, namely:

$$dl_r = dl_l, \quad (7)$$

$$Fl_r = Fl_l. \quad (8)$$

These can be combined into a single matrix equation (similar to [7]), relating the six quantities on the right end to those on the

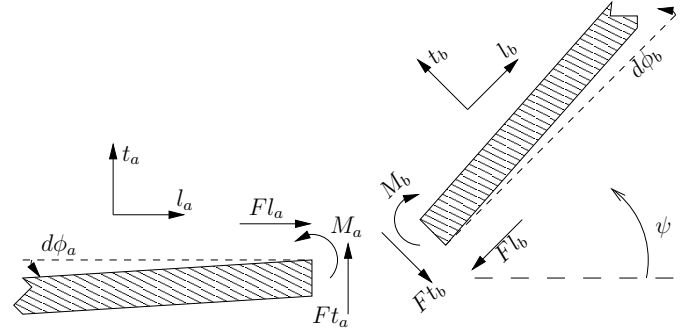


Figure 8. Two simple beams joined together.

left:

$$\begin{pmatrix} dt_r \\ d\phi_r \\ M_r \\ Ft_r \\ dl_r \\ Fl_r \end{pmatrix} = \begin{pmatrix} 1 & l & \frac{l^2}{2EI} & -\frac{l^3}{6EI} & 0 & 0 \\ 0 & 1 & \frac{l}{EI} & -\frac{l^2}{2EI} & 0 & 0 \\ 0 & 0 & 1 & -l & 0 & 0 \\ 0 & 0 & 0 & 1 & 0 & 0 \\ 0 & 0 & 0 & 0 & 1 & 0 \\ 0 & 0 & 0 & 0 & 0 & 1 \end{pmatrix} \begin{pmatrix} dt_l \\ d\phi_l \\ M_l \\ Ft_l \\ dl_l \\ Fl_l \end{pmatrix}. \quad (9)$$

Letting the composite deflection/load vector

$$v = \langle dt, d\phi, M, Ft, dl, Fl \rangle,$$

this can be written

$$v_r = U(l)v_l \leftrightarrow v_r^T = v_l^T U(l)^T. \quad (10)$$

When two beams are rigidly connected, there must be continuity across the interface. In particular, the deflections must be the same at the connected edges, and the forces and moments must balance. If two beams are joined at an angle ψ , as in Fig. 8, the deflection/load vector at the right end of beam a in its l_a/t_a frame must be transformed to the corresponding vector at the left end of beam b in the rotated l_b/t_b frame. The angular displacement $d\phi$ and moment M transform as scalars, and so remain unchanged under rotations as expected. Meanwhile, the displacements $\langle dl, dt \rangle$ and forces $\langle Fl, Ft \rangle$ transform as vectors, and must be rotated as such:

$$\begin{pmatrix} dl_b \\ dt_b \end{pmatrix} = \begin{pmatrix} \cos(\psi) & \sin(\psi) \\ -\sin(\psi) & \cos(\psi) \end{pmatrix} \begin{pmatrix} dl_a \\ dt_a \end{pmatrix}. \quad (11)$$

$$\begin{pmatrix} Fl_b \\ Ft_b \end{pmatrix} = \begin{pmatrix} \cos(\psi) & \sin(\psi) \\ -\sin(\psi) & \cos(\psi) \end{pmatrix} \begin{pmatrix} Fl_a \\ Ft_a \end{pmatrix}. \quad (12)$$

Putting these together yields:

$$v_b = R(\psi)v_a \leftrightarrow v_b^T = v_a^T R(\psi)^T, \quad (13)$$

where $R =$

$$\begin{pmatrix} \cos(\psi) & 0 & 0 & 0 & -\sin(\psi) & 0 \\ 0 & 1 & 0 & 0 & 0 & 0 \\ 0 & 0 & 1 & 0 & 0 & 0 \\ 0 & 0 & 0 & \cos(\psi) & 0 & -\sin(\psi) \\ \sin(\psi) & 0 & 0 & 0 & \cos(\psi) & 0 \\ 0 & 0 & 0 & \sin(\psi) & 0 & \cos(\psi) \end{pmatrix}. \quad (14)$$

It is clear that across a straight interface, the loads and displacements must remain unchanged, and indeed $R(0) = I$. This also demonstrates that $U(l_1)U(l_2) = U(l_1 + l_2)$, as expected.

Using these matrices, the static behavior of any piecewise linear folded beam can be elegantly analyzed. Simply by starting at an end and multiplying the relevant matrices for straight lengths and angled junctions, the first order linear relationships between the deflections and loads at either end of the structure can be found as a 6x6 matrix. Boundary conditions can be introduced as known values in the deflection/load vectors, and the system can be reduced to a lower order equation.

5 TRIFOLD LEG LINKAGE

5.1 Mathematical Analysis

The matrix approach described above can now be used to analytically derive the relationships between F_x , F_z , d_x , and d_z in the trifold beam linkage of Fig. 2. Starting from the base and working along a beam to the foot:

$$v_{foot} = A(l, \theta, d) \cdot v_{base}, \quad (15)$$

where

$$A(\cdot)^T = R(\theta)^T U(l)^T R(90^\circ)^T U(d)^T R(90^\circ)^T U(l)^T \times R(-90^\circ)^T U(d)^T R(-90^\circ)^T U(l)^T R(-\theta)^T \quad (16)$$

$$A(\cdot) = R(-\theta)U(l)R(-90^\circ)U(d)R(-90^\circ) \times U(l)R(90^\circ)U(d)R(90^\circ)U(l)R(\theta). \quad (17)$$

This can be simplified by noting that the transverse and angular displacements of the base, as well as the longitudinal and angular displacements of the foot are zero. Also, overall leg equilibrium and symmetry indicates that the moments, horizontal, and vertical forces are equal at both ends of the linkage. That is,

$$v_{foot} = \begin{pmatrix} dz \\ 0 \\ M_r \\ -F_z \\ 0 \\ -F_x \end{pmatrix}, v_{base} = \begin{pmatrix} 0 \\ 0 \\ M_r \\ -F_z \\ dx \\ -F_x \end{pmatrix}. \quad (18)$$

Thus only five unknowns remain, and three can be solved for in terms of the other two. The required input force F_x , step height d_z , and reaction moment M can then be expressed as linear functions of the weight of the robot and the maximum throw of the comb drives:

$$F_x = \frac{1}{D} [AF_z - (24EI)dx], \quad (19)$$

$$d_z = \frac{1}{D} \left[Adx + \frac{2l^2 d^2 (6l^2 + 14ld + d^2)}{EI} F_z \right], \quad (20)$$

$$M = \frac{1}{D} [(4ld^2(6l + 5d)\cos(\theta) - 6l^2 d(l + 3d)\sin(\theta))F_z - 12EI(2d\cos(\theta) + l\sin(\theta))dx] \quad (21)$$

$$(22)$$

where for convenience

$$A = 12ld^2 \cos(2\theta) - (3l^3 + 6l^2 d - 24ld^2 - 8d^3) \sin(2\theta), \quad (23)$$

$$D = 12ld^2 \sin(2\theta) + (3l^3 + 6l^2 d - 24ld^2 - 8d^3) \cos(2\theta) - 3l^3 - 6l^2 d - 24ld^2 - 8d^3. \quad (24)$$

These relations are complicated, but still reveal some important trends. These trends are made clearer when specific numbers are used. Using a weight of $F_z = 125\mu\text{N}$ per leg linkage, and a base displacement of $dx = 15\mu\text{m}$, these values can be determined for a collection of geometries. These are plotted in Fig. 9 for both $d = 10\mu\text{m}$ and $d = 20\mu\text{m}$ beam spacings. Of immediate note is the significant impact of beam spacing on step height. In fact, for a twenty micron spacing, the vertical stiffness is so low that the leg itself can't support the weight of the robot.

These graphs show the biggest tradeoffs are required force vs. step height as a function of angle, and reaction moment vs. step height as a function of length. Since the comb drives are designed to output $100\mu\text{N}$, an optimal angle of around 55° is seen, with length needing to be chosen based on moment considerations.

5.2 ANSYS Simulation

The validity of this model is explored using simulation of the legs using finite element analysis (FEA). A parameterized 3-D model of the trifold flexural linkage is created in SolidWorks then exported to ANSYS for meshing and analysis. The simulation is carried out using a nonlinear solver to account for possible large deflections or buckling. Comparison with the mathematical analysis above reveals reasonable agreement, generally within 10% as shown in Fig. 10. What is important to note is that the FEA solution yields greater step sizes d_z and lower input forces F_x , and so the mathematical analysis generates a conservative model.

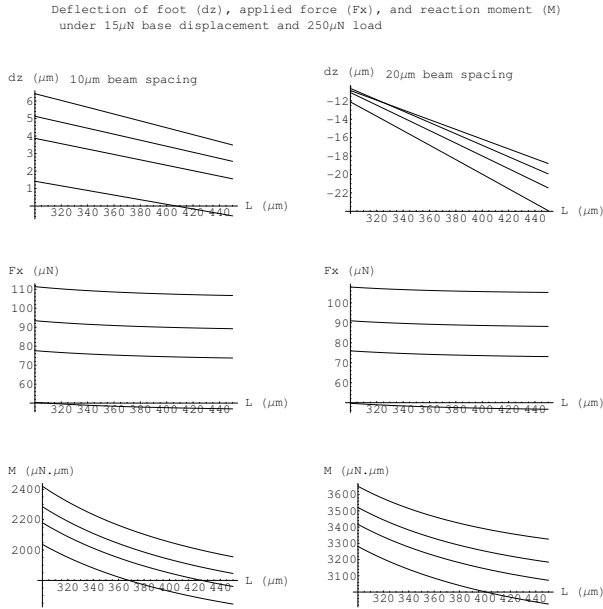


Figure 9. The deflection/load relations are plotted against the geometrical parameters l and θ under a constant base displacement of $15\mu\text{m}$ and load of $250\mu\text{N}$ on the foot. Four values of θ are used, 50° , 55° , 60° , 70° , with 70° being the bottom line on each graph.

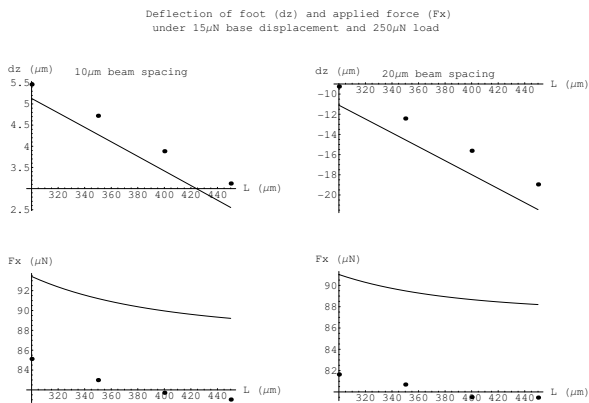


Figure 10. The foot displacement (dz) and applied base force (F_x) are plotted against length l for $\theta = 55^\circ$ under a constant base displacement of $15\mu\text{m}$ and load of $250\mu\text{N}$ on the foot. The line is the analytic model response while the dots are the ANSYS simulation results.

One critical behavior that shows up in the simulation results is the deformed shape of the leg flexure after loading. Both analysis and simulation assume that the serpentine beam elements were independent, in that parallel beams do not interact. However, the simulation results demonstrate that there can be contact between adjacent beams after loading, as in Figs. 11, 12.

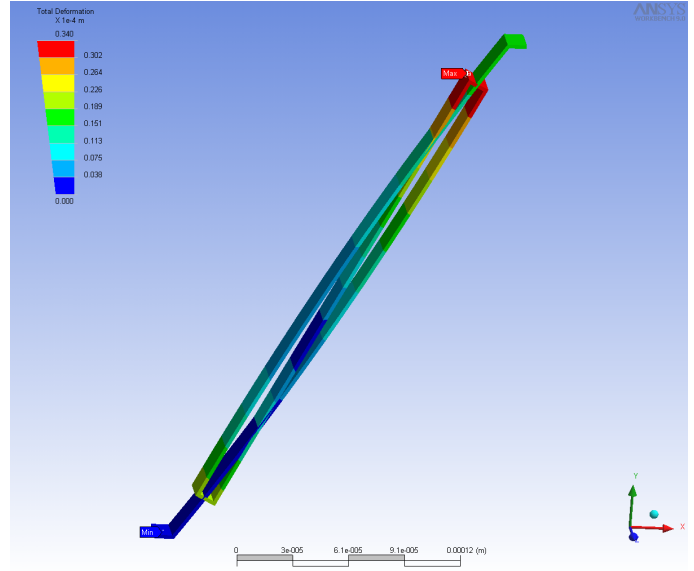


Figure 11. The loaded trifold beam model is deformed through itself, indicating a contact situation.

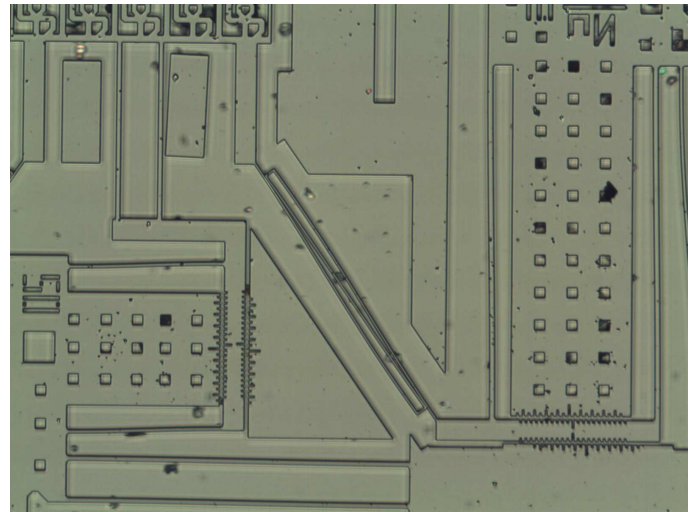


Figure 12. A view of the trifold linkage after loading. The deformed flexure is clearly visible, demonstrating contact between adjacent beams.

5.3 Contact

The contact behavior of a trifold beam can be incorporated into the analytical model through additional force and displacement constraints. A corner collides with an adjacent unconnected edge when their relative transverse displacements sum to the distance between the beams at that point, namely the beam spacing less the width of a beam. Further deflection beyond that point will keep those displacements constrained to sum to that distance. Each beam exerts a force (of equal magnitude) on the

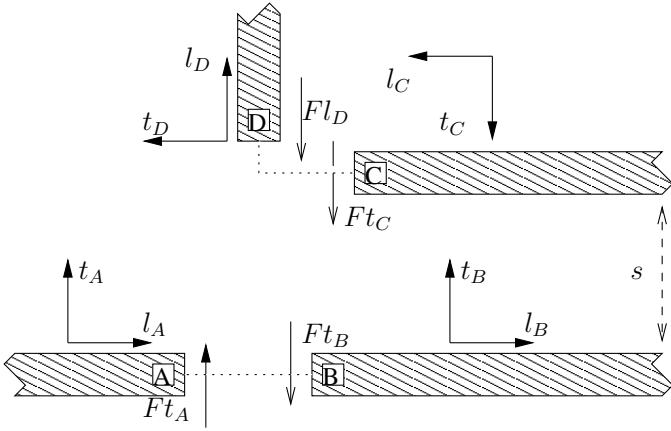


Figure 13. A corner and an adjacent beam could collide.

other beam at that point; this force will be a discontinuity in the force along the beam. That is, across the interface defining the point of contact, the transverse force will differ from one edge to the other in the direction away from the colliding corner.

Consider Fig. 13. If upon deflection, the corner CD contacts the beam at point AB, then the following force and displacement constraints are introduced:

$$dt_A + dt_C = s \quad (25)$$

$$Ft_A + R = Ft_B \quad (26)$$

$$-R - Ft_C = Fl_D \quad (27)$$

Where s is the distance between the beams and R is the force they exert on each other. By labeling the deflection/load vector at all contact points, these constraints can be added in to the set of equations to complete the relationships. Unfortunately this causes the analytic solution to the system to become in general complicated and unwieldy, but the solution can still be used numerically to analyze behavior. The same plots as in Fig. 9 are now shown with contact conditions in 14.

It is interesting to see the difference contact makes on the linkage behavior. The required input force drops slightly while the reaction moment drops significantly. Also, the step size increases drastically. These quantities are uniformly more desirable. Thus, if a design satisfies design requirements using the more tractable no-contact model, the actual device will certainly satisfy the requirements also.

6 PIVOT-BASED LEG LINKAGES

While the flexural legs are necessarily compliant, the ideal legs should be vertically stiff with little rotational resistance. The nonideal nature of the flexural leg linkages are especially evident in the reaction moment generated at the clamped bases of a leg.

Deflection of foot (dz), applied force (Fx), and reaction moment (M) under 15μN base displacement and 250μN load with contact

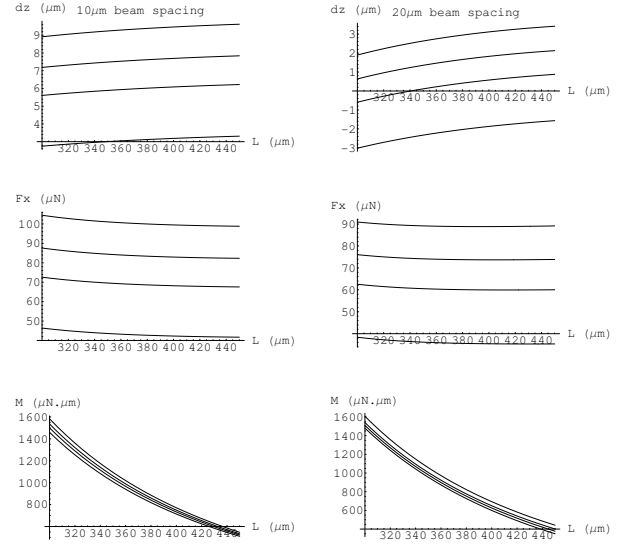


Figure 14. The deflection/load relations are plotted against the geometrical parameters l and $\theta \in \{50^\circ, 55^\circ, 60^\circ, 70^\circ\}$ (with 70° being the bottom line on each graph) under a constant base displacement of $15\mu\text{m}$ and load of $250\mu\text{N}$ on the foot. Contact between adjacent beams is taken into account.

In fact, while a comb drive can generate sufficient force to drive a microrobot, its suspension may twist under large applied moments. This in turn weakens the suspension vertically, potentially resulting in the leg being driven into the substrate under load and rendering it immobile.

An alternate structure was developed to overcome this limitation. In keeping with the one mask SOI process, an enclosed hinge cannot be fabricated. However, a planar cylinder-in-socket joint as in Fig. 3 allows one segment to freely with regards to another. Alternately, to minimize frictional losses arising from the sliding of one surface past the other, a knife edge pivot (Fig. 4) can be used instead. The disjoint sections of either pivot however must be connected to prevent the inner element from escaping the socket out of plane. A long angled folded beam flexure is used for this purpose, providing a restoring force if the cylinder moves out of plane. This flexure also provides a restoring moment as the pivot is rotated. The angular spring constant of this flexure can be determined in much the same way as the above analysis.

7 CONCLUSION

Using the analytical framework built on a matrix formulation of Euler-Bernoulli beam theory, the performance of a class of two degree-of-freedom walking legs was quantified. First order analysis results proved to be more conservative than FEA

simulation or the more refined model including contact behavior, and so was used as a loose bound for estimating behavior. Using these three methods, it was demonstrated that driving a walking microrobot with flexural legs is a feasible goal. A parallel development track with pivot-based legs also was shown to be promising. The next step will of course be to test the structures analyzed in this paper.

REFERENCES

- [1] Donald, B., Levey, C., McGray, C., Paprotny, I., and Rus, D., 2006. “An untethered, electrostatic, globally controllable MEMS micro-robot”. *Journal of Microelectromechanical Systems*, **15**(1), pp. 1–15.
- [2] Lindsay, L., Teasdale, D., Milanovic, V., Pister, K., and Pello, C., 2001. “Thrust and electrical power from solid propellant microrockets”. In Proc. 1Jth Annual Int. Conf. on Microelectromechanical Systems (MEMS 2001), pp. 606–610.
- [3] Scarfogliero, U., Stefanini, C., and Dario, P., 2006. “A bioinspired concept for high efficiency locomotion in micro robots: the jumping robot grillo”. In Robotics and Automation, 2006. ICRA 2006. Proceedings 2006 IEEE International Conference on, pp. 4037–4042.
- [4] Hollar, S., Flynn, A., Bergbreiter, S., and Pister, K., 2005. “Robot leg motion in a planarized-SOI, two-layer polysi process”. *Journal of Microelectromechanical Systems*, **14**(4), pp. 725–740.
- [5] Last, M., Subramaniam, V., and Pister, K., 2005. “Out of plane motion of assembled microstructures using a single-mask SOI process”. In Solid-State Sensors, Actuators and Microsystems, 2005. Digest of Technical Papers. TRANSDUCERS '05. The 13th International Conference on, Vol. 1, pp. 684–687.
- [6] Tung, Y.-C., and Kurabayashi, K., 2005. “A single-layer pdms-on-silicon hybrid microactuator with multi-axis out-of-plane motion capabilities”. *JMEMS*, **14**(3), June, pp. 548–566.
- [7] Khattak, A., Garvey, S., and Popov, A., 2006. “Repeated resonances in folded-back beam structures”. *Journal of sound and vibration*, **290**(1-2), February, pp. 309–320.